Analytical integration of the tractions induced by non-singular dislocations on an arbitrary shaped triangular quadratic element.

Sylvain Queyreau[1], **Khiem Hoang**[1], **Xiangjun Shi**[1]

[1]LSPM CNRS UPR 3407, Université Paris 13, Sorbonne-Paris-Cité, 93430, Villetaneuse, France

E-mail: sylvain.queyreau@cnrs.fr

Sylvie Aubry[2], **Athanasios Arsenlis**[2]

Lawrence Livermore National Laboratory, P. O. Box 808, Livermore, California 94551, USA

Abstract. An analytical model is proposed to evaluate the nodal force induced by a segment of dislocation upon an arbitrary shaped triangular element. This calculation is required in hybrid methods that associate Dislocation Dynamics to Boundary or Finite Element to solve simultaneously the evolution of large ensembles of dislocations with complexe boundary conditions. Nodal forces are defined as the triple integration of the unbalanced traction field induced by a straight dislocation upon the surface of the element. Following our previous approach [Queyreau et al. MSMSE 2014] on a simpler geometry and in the case of linear isotropic elasticity, triple integrals are solved by sequences of integration by parts that exhibit recurrence relations. The traction field is defined and finite everywhere even at the core of dislocations, thanks to the use of the non-singular stress expression formulated by Cai and coworkers [Cai et al. JMPS 2006]. A solution is also proposed for the case of a semi-infinite segment through the study of the asymptotic behaviour of the analytical expressions. The proposed approach is exact and very efficient computationally. The choice of an arbitrary shaped triangular element and quadratic shape functions allow to consider the most complex geometries and comply with automatic meshing procedures. These analytical expressions could also be employed to estimate dislocation interactions with interfaces.

PACS numbers: 00.00, 20.00, 42.10

Keywords: Article preparation, IOP journals Submitted to: *Modelling Simulation Mater. Sci. Eng.*

1. Introduction

Hybrid methods -associating Dislocation Dynamics (DD) with Boundary (BE), Finite Elements (FE) or spectral methods- have been formulated two decades ago to solve simultaneously the evolution of complexe dislocation ensembles with prescribed boundary conditions [1, 2, 3, 4, 5, 6, 7, 8, 9]. Some typical examples of applications concern polycristalline plasticity [1, 10], plasticity in finite domain [3, 11, 12], or heterogeneous materials in the presence of second phases [8, 13]. Most of these approches rely on the superposition principle [1] and linear elasticity. The stress field solution is decomposed into a "classical" field associated to dislocations in an infinite medium and a corrective stress field that enforces the prescribed boundary conditions at the internal or external boundaries of the simulated domain.

Solving the corrective field using FE/BE require the evaluation of the unbalanced tractions induced by dislocations at the boundaries of the domain [14, 15]. These unbalanced tractions exist because DD relies on analytical expressions of the elastic fields of dislocations in an infinite and homogeneous domain, which allows for a rapid and accurate evaluation of dislocation-dislocation interactions. In the case of free surfaces, for example, the unbalanced tractions are then reverted and constitute inputs to the associated boundary value problem solved by FE/BE. Formally, the tractions $\sigma \cdot \mathbf{n}$ are expressed as the triple integration of the infinite domain stress field σ along the dislocation line and over the surface element of normal $\mathbf{n}$. Tractions are then projected and appropriately distributed as nodal forces $\mathbf{F}^{(n)}$ over the nodes of the surface element by means of shape functions:

$$\mathbf{F}^{(n)} = \int_{S^{(E)}} [\sigma^{\infty}(\mathbf{x}) \cdot \mathbf{n}] \, N^{(n)}(\mathbf{x}) \, dS \tag{1}$$

This constitutes arguably the most demanding task when coupling DD to FE/BE as traction evaluation must be carried out over all segments of the simulated microstructure and on all surface elements delimiting the domain [14, 11]. Conventional numerical integration could be employed to evaluate tractions, but care should then be paid to the evaluation and control of the associated numerical errors since they will directly alter the accuracy of the FE/BE resolution [16]. In addition, the inverse dependence of the dislocation stress field with respect to distance is not particularly well adapted to, say, Gauss-Legendre quadratures, which leads to very large numerical errors when the dislocations are close to the surfaces. Singularities near the core of dislocations that are typical of classical theory of dislocations can also induce dramatic errors [14].

In a previous work [16], the present authors showed that it is possible to derive fully analytical expressions for the tractions induced by a segment of dislocation on a basic quadrangle surface element and in the case of linear isotropic elasticity. The set of required triple integrals was obtained by a series of successive integrations by parts exhibiting recurrence relationships. Thanks to the use of the non-singular theory of dislocation proposed by Cai and collaborators [17], the traction field is defined

everywhere in space, even in the case of a segment piercing the surface element. As a result, this analytical formalism was found to be exact and numerically competitive when compared to classical quadrature strategies, but suffered from a couple of limitations. The first limitation is related to the use of linear shape functions that may not capture the strong local spatial variations of the field being solved by FE. Linear shape functions are also associated to volume or surface elements with fewer degrees of freedom. Another limitation has to do with the rectangular geometry used for the surface element that considerably limits the geometry complexity of the domain being investigated.

The approach was recently extended to the case of anisotropic linear elasticity in [18]. Closed-form analytical expressions of the stress field around a dislocation do not exist in anisotropic elasticity, but the required derivatives of the Green's function can be expressed as angular integrals around the dislocation segment [19]. As in [20], these integrals are evaluated by means of a spherical harmonics expansion whose truncation order can be adapted to meet the imposed accuracy. Thanks to the expression of the spherical harmonics, the nodal force induced by dislocation remains in the form of (sums of) triple integrals of ratios of polynomials whose variables are spanning only the dislocations and the surface element. The solution is still obtained by recurrence relations derived from integration by parts, providing a fast and accurate evaluation algorithm. The surface element geometry was also limited to a simple linear quadrangle.

In this paper, we extend our previous work and derive analytical expressions of the tractions induced by dislocations to the case of arbitrary shaped quadratic triangular element. This new surface geometry complies with elements associated with more degrees of freedom and also constitutes a very versatile geometry as it can mesh any given 3D geometry and is suitable for adaptative mesh refinement methods. The model still relies on sequences of integration by parts, but new sets of integrals are introduced. We will see that higher order shape functions involve additional integrals to be solved. The double integral over a now triangular element, changes the definition of the integral bounds, which makes integration order important. The new formalism retains the main advantage of our previous work as nodal forces are exact, numerically efficient, and the traction field is defined everywhere in the domain including at the core of dislocations and in the case of piercing segments. We also offer a specific solution for semi-infinite segments that can be employed to virtually "close" the dislocation microstructure.

The paper is organised as follows. The first section sets out the theoretical background of this work. The next section presents our analytical approach for finite and semi-infinite segments of dislocations. Finally, the paper ends with a comparison with a conventional numerical evaluation of tractions and a short discussion. For the sake of clarity, the mathematical details of our method are left in the appendix.

2. Method

In an infinite and homogeneous linear elastic medium, the stress field induced by a dislocation loop $\sigma^{\infty}(\mathbf{x})$ at a point $\mathbf{x}$ is expressed as a contour integral along the loop

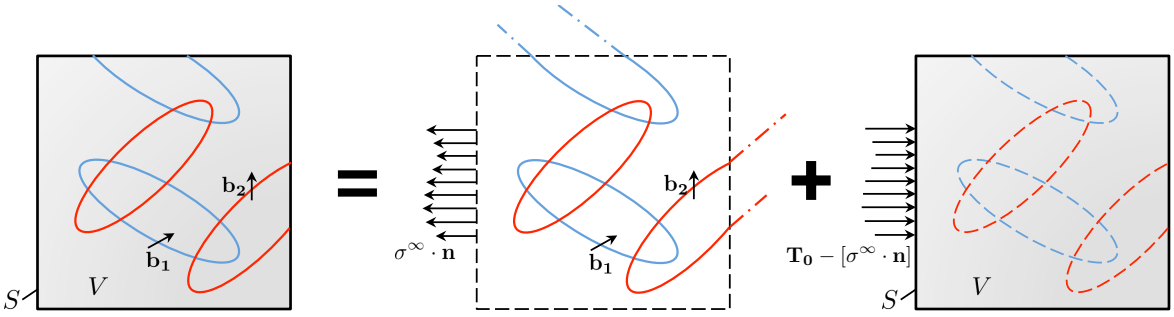

Figure 1. Illustration of hybrid method solve from [16] (a). Two slip families of Burgers vectors $\mathbf{b_1}$ and $\mathbf{b_2}$ are present in a Bicrystal V, bounded by S. (b) The traction field due to the discrete dislocation ensemble in the infinite domain is evaluated on the domain boundary. This calculation accounts for dislocations contained within the domain and virtual segments used to close open dislocation loops. (c) Then, a FE or BE simulation of a non-dislocated elastic medium gives the corrective stress field that enforce the prescribed boundary conditions.

[19] as:

$$\sigma_{ij}^{\infty}(\mathbf{x}) = C_{ijkl} \oint \epsilon_{lnh}\, C_{pqmn}\, \frac{\partial G_{kp}(\mathbf{x}-\mathbf{x}')}{\partial x_q}\, b_m\, dx'_h \tag{2}$$

Where $\mathbf{b}$ the Burgers vector of the loop, $\mathbf{x}'$ is a second coordinate that runs along the dislocation. C_{ijkl} is the elastic stiffness matrix of the medium, and ϵ_{lnh} the permutation operator. $G_{kp}(\mathbf{x}-\mathbf{x}')$ are the Green's functions of elasticity and correspond to the displacement component in the x_k direction at point $\mathbf{x}$ due to a body force placed at $\mathbf{x}'$ in the x_p direction [19]. In conventional theory of dislocations, the well-known singularity of the stress field close to the dislocation core is due to the sharp (Dirac) distribution of Burgers vectors used to obtain the stress field. To remove the singularity, Cai et al. [17] replaced the sharp Burgers distribution by an isotropic spreading function. While other solutions have been proposed to remove the singularity of stress expressions at the core of dislocations [21], Cai et al. [17] approach remain very attractive in the context of DD applications with only one additional parameter defined as the core spreading a, classically taken as $||\mathbf{b}||$, and expressions for the stress, self energy and interacting forces of dislocations are fully analytical in the case of linear isotropic medium. The Green's functions become in the case of linear elasticity:

$$G_{ij}(\mathbf{x}-\mathbf{x}') = \frac{1}{8\pi\mu}\left[\delta_{ij}\partial_p\partial_p - \frac{1}{2(1-\nu)}\partial_i\partial_j\right] R_a \tag{3}$$

where μ and ν the isotropic shear modulus and Poisson's ratio, respectively. The metric R is defined as $||\mathbf{x}-\mathbf{x}'||$ and R_a is the convolution of R with the Burgers distribution. Thanks to the choice of spreading function R_a simply reads $\sqrt{R_K^2+a^2}$. When integrating equation 2 along a straight segment delimited by nodes $\mathbf{x_1}$ and $\mathbf{x_2}$, the stress field can now be rewritten as:

$$\sigma^{(x_1x_2)}(\mathbf{x}) = -\frac{\mu}{8\pi}\int_{\mathbf{x}_1}^{\mathbf{x}_2}\left(\frac{2}{R_a^3}+\frac{3a^2}{R_a^5}\right)[(\mathbf{R}\times\mathbf{b})\otimes d\mathbf{x}' + d\mathbf{x}'\otimes(\mathbf{R}\times\mathbf{b})]$$

$$+\frac{\mu}{4\pi\,(1-\nu)}\int_{\mathbf{x}_1}^{\mathbf{x}_2}\left(\frac{1}{R_a^3}+\frac{3a^2}{R_a^5}\right)\left[(\mathbf{R}\times\mathbf{b})\cdot d\mathbf{x}'\right]\mathbf{I}_2$$
$$-\frac{\mu}{4\pi\,(1-\nu)}\int_{\mathbf{x}_1}^{\mathbf{x}_2}\frac{1}{R_a^3}\left((\mathbf{b}\times d\mathbf{x}')\otimes\mathbf{R}+\mathbf{R}\otimes(\mathbf{b}\times d\mathbf{x}')\right)$$
$$+\frac{\mu}{4\pi\,(1-\nu)}\int_{\mathbf{x}_1}^{\mathbf{x}_2}\frac{3}{R_a^5}\left[(\mathbf{R}\times\mathbf{b})\cdot d\mathbf{x}'\right]\mathbf{R}\otimes\mathbf{R} \tag{4}$$

where the superscript refers to the nodes identity. It can be noted that when comparing to conventional (singular) theory of dislocation, few additional terms can be seen and correspond to higher powers of $1/R_a$. Obviously, as a goes to 0, the classical singular stress expressions are recovered.

When the dislocated domain is finite or in presence of internal interfaces, the stress field derived for the infinite domain induce a non-zero traction field defined as $\mathbf{T}(\mathbf{x}) = \sigma^{\infty}\cdot\mathbf{n}$ at the surfaces of interfaces of the domain, where $\mathbf{n}$ is their normal. In the context of hybrid DD - FE or BE solver [1, 15], 1) these unbalanced tractions must be evaluated, and appropriately transformed into a set of nodal forces at the nodes of these surface elements used by BE or FE. 2) The classical set of elasticity equations is solved using FE or BE to obtain the corrective (or image) displacement field enforcing proper boundary conditions: zero traction condition for free surface and no traction jump across internal interfaces. 3) Finally, the corrective stress field obtained by FE or BE is transformed into a Peach and Koehler Force and applied in return to the segment of dislocations.

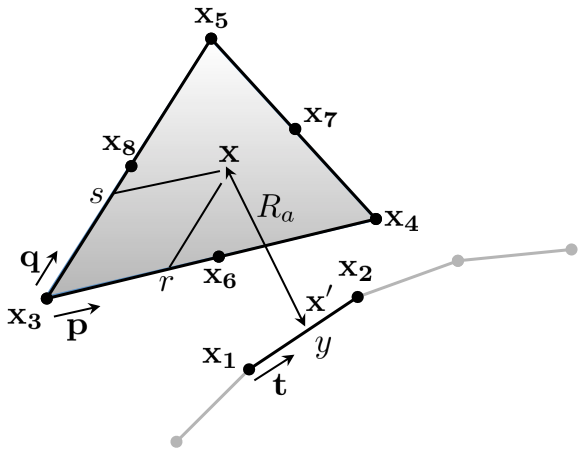

Figure 2. Geometry under consideration and definition of the variables to be used.

The traction field is transformed into a nodal force at a node $\mathbf{n}$ of a surface element E [22] by:

$$\mathbf{F}^{(n)} = \int_{S^{(E)}}\left[\sigma^{\infty}(\mathbf{x})\cdot\mathbf{n}\right]N^{(n)}(\mathbf{x})\,dS \tag{5}$$

where, $S^{(E)}$ is the area of the element and $N^{(n)}$ the associated shape function. In this paper, we focus on an arbitrary shaped six node element with quadratic shape functions

[22]. The corresponding geometry is given in figure 2. The vertices of the triangular element are defined by the Carthesian coordinates $\mathbf{x_3}$, $\mathbf{x_4}$ and $\mathbf{x_5}$. Coordinate $\mathbf{x}'$ spans the surface element. We introduce a new (non orthogonal) basis of vectors $\mathbf{p} = \frac{\mathbf{x_3x_4}}{||\mathbf{x_3x_4}||}$, $\mathbf{q} = \frac{\mathbf{x_3x_5}}{||\mathbf{x_3x_5}||}$ on the surface of the element, and $\mathbf{t} = \frac{\mathbf{x_1x_2}}{||\mathbf{x_1x_2}||}$. We can rewrite the distance vector $\mathbf{R}$ as $\mathbf{R} = r\mathbf{p} + s\mathbf{q} + t\mathbf{y}$. r, s and t are now scalars spanning the surface and the dislocation. This decomposition is valid for all orientation of $\mathbf{p}$ and $\mathbf{q}$ ($\mathbf{p}\cdot\mathbf{q} < 1$) but is undetermined when the segment is parallel to the surface: $\mathbf{t}\cdot(\mathbf{p}\times\mathbf{q}) \neq 0$. The infinitesimal parallelogram element dS equals $\sin(\mathbf{p},\mathbf{q})drds$

Here, we choose to use quadratic shape functions [22]. We introduce area coordinates of $\mathbf{x}$ with respect to the vertices $\mathbf{x_3}$, $\mathbf{x_4}$ and $\mathbf{x_5}$ as $L_1 = \frac{r-r_1}{r_2-r_1}$, $L_2 = \frac{s-s_1}{s_2-s_1}$ and $L_3 = 1 - L_1 - L_2$. Taking node $\mathbf{x_3}$ and node $\mathbf{x_6}$ as examples for corner and midside nodes, respectively, the nodal forces are: $N^{(3)} = L_3(2L_3 - 1)$ and $N^{(6)} = 4L_1L_3$. By Replacing the definition of $L_{(n)}$, the quadratic interpolation functions become:

$$N^{(3)} = \frac{2}{L_p^2}r^2 + \frac{2}{L_q^2}s^2 + \frac{4}{L_pL_q}rs - \left(\frac{4r_1}{L_p^2} + \frac{3}{L_p} + \frac{4s_1}{L_pL_q}\right)r - \left(\frac{4s_1}{L_q^2} + \frac{3}{L_q} + \frac{4r_1}{L_pL_q}\right)s \quad (6)$$

$$N^{(6)} = -\frac{4}{L_p^2}r^2 - \frac{4}{L_pL_q}rs + 4\left(\frac{1}{L_p} + \frac{2r_1}{L_p^2} + \frac{s_1}{L_pL_q}\right)r + \frac{4r_1}{L_pL_q}s - 4\left(\frac{r_1}{L_p} + \frac{r_1^2}{L_p^2} + \frac{r_1s_1}{L_pL_q}\right) \quad (7)$$

The interpolation functions for the other nodes can be seen in Appendix A.

By inserting the non-singular stress expression Eq. 4 into the nodal force expression of Eq. 5, and recalling the definition $\mathbf{R} = r\mathbf{p} + s\mathbf{q} + t\mathbf{y}$, one obtains:

$$\begin{aligned}
\mathbf{F}^{(n)} = {} & \frac{\mu\alpha}{8\pi}\left\{(\mathbf{t}\times\mathbf{b})(\mathbf{t}\cdot\mathbf{n}) + \mathbf{t}\left[(\mathbf{t}\times\mathbf{b})\cdot\mathbf{n}\right]\right\}\int_{r_1}^{r_2}\int_{s_1}^{s_2}\int_{y_1}^{y_2}\left(\frac{2}{R_a^3} + \frac{3a^2}{R_a^5}\right)yN^{(n)}(r,s)dsdrdy \\
& + \frac{\mu\alpha}{8\pi}\left\{(\mathbf{p}\times\mathbf{b})(\mathbf{t}\cdot\mathbf{n}) + \mathbf{t}\left[(\mathbf{p}\times\mathbf{b})\cdot\mathbf{n}\right]\right\}\int_{r_1}^{r_2}\int_{s_1}^{s_2}\int_{y_1}^{y_2}\left(\frac{2}{R_a^3} + \frac{3a^2}{R_a^5}\right)r\,N^{(n)}(r,s)\,dsdr \\
& + \frac{\mu\alpha}{8\pi}\left\{(\mathbf{q}\times\mathbf{b})(\mathbf{t}\cdot\mathbf{n}) + \mathbf{t}\left[(\mathbf{q}\times\mathbf{b})\cdot\mathbf{n}\right]\right\}\int_{r_1}^{r_2}\int_{s_1}^{s_2}\int_{y_1}^{y_2}\left(\frac{2}{R_a^3} + \frac{3a^2}{R_a^5}\right)s\,N^{(n)}(r,s)\,dsd \\
& - \frac{\mu\alpha}{4\pi(1-\nu)}\left[(\mathbf{p}\times\mathbf{b})\cdot\mathbf{t}\right]\mathbf{n}\int_{r_1}^{r_2}\int_{s_1}^{s_2}\int_{y_1}^{y_2}\left(\frac{1}{R_a^3} + \frac{3a^2}{R_a^5}\right)r\,N^{(n)}(r,s)\,dsdrdy \\
& - \frac{\mu\alpha}{4\pi(1-\nu)}\left[(\mathbf{q}\times\mathbf{b})\cdot\mathbf{t}\right]\mathbf{n}\int_{r_1}^{r_2}\int_{s_1}^{s_2}\int_{y_1}^{y_2}\left(\frac{1}{R_a^3} + \frac{3a^2}{R_a^5}\right)s\,N^{(n)}(r,s)\,dsdrdy \\
& + \frac{\mu\alpha}{4\pi(1-\nu)}\left\{(\mathbf{b}\times\mathbf{t})(\mathbf{t}\cdot\mathbf{n}) + \mathbf{t}\left[(\mathbf{b}\times\mathbf{t})\cdot\mathbf{n}\right]\right\}\int_{r_1}^{r_2}\int_{s_1}^{s_2}\int_{y_1}^{y_2}\frac{1}{R_a^3}y\,N^{(n)}(r,s)\,dsdrdy \\
& + \frac{\mu\alpha}{4\pi(1-\nu)}\mathbf{p}\left[(\mathbf{b}\times\mathbf{t})\cdot\mathbf{n}\right]\int_{r_1}^{r_2}\int_{s_1}^{s_2}\int_{y_1}^{y_2}\frac{1}{R_a^3}r\,N^{(n)}(r,s)\,dsdrdy \\
& + \frac{\mu\alpha}{4\pi(1-\nu)}\mathbf{q}\left[(\mathbf{b}\times\mathbf{t})\cdot\mathbf{n}\right]\int_{r_1}^{r_2}\int_{s_1}^{s_2}\int_{y_1}^{y_2}\frac{1}{R_a^3}s\,N^{(n)}(r,s)\,dsdrdy \\
& - \frac{\mu\alpha}{4\pi(1-\nu)}\left[(\mathbf{p}\times\mathbf{b})\cdot\mathbf{t}\right](\mathbf{t}\cdot\mathbf{n})\,\mathbf{p}\int_{r_1}^{r_2}\int_{s_1}^{s_2}\int_{y_1}^{y_2}\frac{3}{R_a^5}r^2y\,N^{(n)}(r,s)\,dsdrdy \\
& - \frac{\mu\alpha}{4\pi(1-\nu)}\left[(\mathbf{q}\times\mathbf{b})\cdot\mathbf{t}\right](\mathbf{t}\cdot\mathbf{n})\,\mathbf{q}\int_{r_1}^{r_2}\int_{s_1}^{s_2}\int_{y_1}^{y_2}\frac{3}{R_a^5}s^2y\,N^{(n)}(r,s)\,dsdrdy
\end{aligned}$$

$$
\begin{aligned}
&- \frac{\mu\alpha}{4\pi\,(1-\nu)}\left[(\mathbf{p}\times\mathbf{b})\cdot\mathbf{t}\right](\mathbf{t}\cdot\mathbf{n})\,\mathbf{t}\int_{r_1}^{r_2}\int_{s_1}^{s_2}\int_{y_1}^{y_2}\frac{3}{R_a^5}ry^2\,N^{(n)}(r,s)\,dsdrdy\\
&- \frac{\mu\alpha}{4\pi\,(1-\nu)}\left[(\mathbf{q}\times\mathbf{b})\cdot\mathbf{t}\right](\mathbf{t}\cdot\mathbf{n})\,\mathbf{t}\int_{r_1}^{r_2}\int_{s_1}^{s_2}\int_{y_1}^{y_2}\frac{3}{R_a^5}sy^2\,N^{(n)}(r,s)\,dsdrdy\\
&- \frac{\mu\alpha}{4\pi\,(1-\nu)}\left[(\mathbf{p}\times\mathbf{b})\cdot\mathbf{t}\right](\mathbf{t}\cdot\mathbf{n})\,\mathbf{q}\int_{r_1}^{r_2}\int_{s_1}^{s_2}\int_{y_1}^{y_2}\frac{3}{R_a^5}rsy\,N^{(n)}(r,s)\,dsdrdy\\
&- \frac{\mu\alpha}{4\pi\,(1-\nu)}\left[(\mathbf{q}\times\mathbf{b})\cdot\mathbf{t}\right](\mathbf{t}\cdot\mathbf{n})\,\mathbf{p}\int_{r_1}^{r_2}\int_{s_1}^{s_2}\int_{y_1}^{y_2}\frac{3}{R_a^5}rsy\,N^{(n)}(r,s)\,dsdrdy
\end{aligned}
$$

Next, we will show that it is possible to derive a fully analytical expression for the nodal force $\mathbf{F}^{(n)}$ on an arbitrary-shaped triangular element.

3. Results and discussions

Derivation of analytical expressions

When inserting the quadratic shape functions 6 or 7 into the nodal force expression 8, one can see that expressing $\mathbf{F}^{(n)}$ requires to solve 55 triple integrals of the form:

$$
\begin{aligned}
&H_{ijk-l} = \iiint \frac{r^i s^j y^k}{R_a^l} dr ds dy \\
&\text{with } l \text{ integer } = 3 \text{ or } 5 \\
&\text{and } i,j,k \text{ integers} \in [0,5]
\end{aligned}
\tag{9}
$$

In the case of the triangular element, the metric $R_a = \sqrt{R_k R_k + a^2}$ is now expressed as:

$$
R_a^2 = y^2 + r^2 + s^2 + 2y(cr + ds) + 2ers + a^2 \tag{10}
$$

where $c = \mathbf{p}\cdot\mathbf{t}$, $d = \mathbf{q}\cdot\mathbf{t}$ and $e = \mathbf{p}\cdot\mathbf{q}$. Following our previous work [16], triple integrals 9 can be analytically derived by a series of integration by parts that exhibit recurrence relations. However, due to the presence of the 'cross' term ers when $\mathbf{p}\cdot\mathbf{q} \neq 0$, none of the expressions derived for the linear quadrangle can be reused here, and an entirely new solution must be derived. We start with the partial derivatives of $\frac{r^i s^j y^k}{R_a^l}$:

$$
\frac{\partial}{\partial r}\frac{r^i s^j y^k}{R_a^l} = i\frac{r^{i-1} s^j y^k}{R_a^l} - l\frac{r^i s^j y^k}{R_a^{l+2}}[r + cy + es] \tag{11}
$$

$$
\frac{\partial}{\partial s}\frac{r^i s^j y^k}{R_a^l} = j\frac{r^i s^{j-1} y^k}{R_a^l} - l\frac{r^i s^j y^k}{R_a^{l+2}}[s + dy + er] \tag{12}
$$

$$
\frac{\partial}{\partial y}\frac{r^i s^j y^k}{R_a^l} = k\frac{r^i s^j y^{k-1}}{R_a^l} - l\frac{r^i s^j y^k}{R_a^{l+2}}[y + cr + ds] \tag{13}
$$

The first term in the right hand side of these equations are obviously present when $i \geqslant 1$, $j \geqslant 1$ or $k \geqslant 1$. Three successive integrations over r, s and y leads to:

$$
\iiint \frac{\partial}{\partial r}\frac{r^i s^j y^k}{R_a^l} = i\iiint \frac{r^{i-1} s^j y^k}{R_a^l} - l\iiint \frac{r^{i+1} s^j y^k}{R_a^{l+2}} - cl\iiint \frac{r^i s^j y^{k+1}}{R_a^{l+2}} - el\iiint \frac{r^i s^{j+1} y^k}{R_a^{l+2}} \tag{14}
$$

$$\iiint \frac{\partial}{\partial s}\frac{r^i s^j y^k}{R_a^l} = i\iiint \frac{r^i s^{j-1} y^k}{R_a^l} - l\iiint \frac{r^i s^{j+1} y^k}{R_a^{l+2}} - dl\iiint \frac{r^i s^j y^{k+1}}{R_a^{l+2}} - el\iiint \frac{r^{i+1} s^j y^k}{R_a^{l+2}} \tag{15}$$

$$\iiint \frac{\partial}{\partial y}\frac{r^i s^j y^k}{R_a^l} = i\iiint \frac{r^i s^j y^{k-1}}{R_a^l} - l\iiint \frac{r^i s^j y^{k+1}}{R_a^{l+2}} - cl\iiint \frac{r^{i+!} s^j y^k}{R_a^{l+2}} - dl\iiint \frac{r^i s^{j+1} y^k}{R_a^{l+2}} \tag{16}$$

(17)

Assuming that double and lower-orders triple integrals are known from previous iterations, these expressions provide a set of linear equations for three unknowns that are higher-order triple integrals $\iiint \frac{r^i s^{j+1} y^k}{R_a^{l+2}}$, $\iiint \frac{r^i s^{j+1} y^k}{R_a^{l+2}}$ and $\iiint \frac{r^i s^{j+1} y^k}{R_a^{l+2}}$. These integrals will be evaluated at the different bounds r_1, r_f, s_1, s_f, y_1 and y_2.

Two additional complications associated to the triangular geometry are associated with the upper bounds r_f and s_f for the r and s integrals that are not constant any more, but depend upon the value of s and r, respectively. Indeed, Figure 2 shows that the upper bound s_f linearly increases with r and reaches a maximum at vertice $\mathbf{x_4}$ with a value s_2. Consequently, the order in the successive integration over r and s is now important, and two solutions must be derived for double integrals $\iint \frac{r^i s^j y^k}{R_a^l} dr dy$ assuming s integration was done first, and for double integrals $\iint \frac{r^i s^j y^k}{R_a^l} ds dy$ when r integration was required first. For example, the partial derivation 11 over r imposes to start with an integration over r, which introduces bound $r_f(s)$ that is function of s, and only then we can proceed to the integration over s:

$$\Big[\frac{r^i s^j y^k}{R_a^l}\Big]_{r_1}^{r_f=fct(s)} = i\int \frac{r^{i-1} s^j y^k}{R_a^l} dr - l\int \frac{r^i s^j y^k}{R_a^{l+2}}[r + cy + es]dr \tag{18}$$

upper bound $r_f(s)$ can be expressed as:

$$r_f(s) = -\frac{r_2 - r_1}{s_2 - s_1}(s - s_1) + r_2 \tag{19}$$

that we can rewrite in a more compact form as $r_f(s) = fs + g$. Continuing with the subsequent integrations over s and y leads to:

$$\iint \frac{(fs+g)^i s^j y^k}{R_a^l[r_f]} ds dy - r_1^i \iint \frac{s^j y^k}{R_a^l[r_1]} ds dy = i\iint \frac{r^{i-1} s^j y^k}{R_a^l} dr ds dy - l\iiint \frac{r^i s^j y^k}{R_a^{l+2}}[r + cy +$$

The three solutions of the system of equations can finally be expressed as a function of lower-order triple integrals and double integrals (see Appendixes A for details):

$$\begin{aligned} H_{ij(k+1)(l+2)} = \frac{1}{l(1-c^2-d^2-e^2+2cde)}\Big\{ & (1-e^2)[kH_{ij(k-1)l} - y^k D_{ijl}] - i(c-de)H_{(i-1)jk} \\ & - j(d-ce)H_{i(j-1)kl} + (c-de)\Big[\iint \frac{(fs+g)^i s^j y^k}{R_a^l[r_f]} ds dy - r_1^i \iint \frac{s^j y^k}{R_a^l[r_1]} ds dy \\ & + (d-ce)\Big[\iint \frac{r^i (hr+m)^j y^k}{R_a^l[s_f]} dr dy - s_1^j \iint \frac{r^i y^k}{R_a^l[s_1]} dr dy\Big]\Big\} \end{aligned} \tag{21}$$

$$\begin{aligned} H_{(i+1)jk(l+2)} = \frac{1}{l(1-e^2)}\Big\{ & iH_{(i-1)jkl} - ejH_{i(j-1)kl} - l(c-de)H_{ij(k+1)(l+2)} \\ & - \Big[\iint \frac{(fs+g)^i s^j y^k}{R_a^l[r_f]} ds dy - r_1^i \iint \frac{s^j y^k}{R_a^l[r_1]} ds dy\Big] \end{aligned}$$

$$+ e\Big[\iint \frac{r^i(hr+m)^j y^k}{R_a^l[s_f]}drdy - s_1^j \iint \frac{r^i y^k}{R_a^l[s_1]}drdy\Big]\Big\} \tag{22}$$

$$\begin{aligned} H_{i(j+1)k(l+2)} = \frac{1}{l(1-e^2)}\Big\{ & jH_{i(j-1)kl} - eiH_{(i-1)jkl} - l(d-ce)H_{ij(k+1)(l+2)} \\ & - \Big[\iint \frac{r^i(hr+m)^j y^k}{R_a^l[s_f]}drdy - s_1^j \iint \frac{r^i y^k}{R_a^l[s_1]}drdy\Big] \\ & + e\Big[\iint \frac{(fs+g)^i s^j y^k}{R_a^l[r_f]}dsdy - r_1^i \iint \frac{s^j y^k}{R_a^l[r_1]}dsdy\Big]\Big\} \end{aligned} \tag{23}$$

$$\begin{aligned} H_{ijk(l+2)} = \frac{1}{la^2}\Big[& (l-i-j-k-3)H_{ijkl} + y^k D_{ijl} \\ & + \iint \frac{r^i(hr+m)^j y^k}{R_a^l[s_f]}drdy - s_1^j \iint \frac{r^i y^k}{R_a^l[s_1]}drdy \\ & + \iint \frac{(fs+g)^i s^j y^k}{R_a^l[r_f]}dsdy - r_1^i \iint \frac{s^j y^k}{R_a^l[r_1]}dsdy\Big] \end{aligned} \tag{24}$$

A similar methodology can be applied to derive a recurrence relations for double integrals as a function of single integrals, and finally to derive the recurrence relations for single integrals. Ultimately, few low order integrals cannot be obtained by recurrence relations and need to be solved analytically. This concerns the following seed integrals:

$$\begin{aligned} & \iiint \frac{1}{R_a^3}drdsdy,\ \iint \frac{1}{R_a^3}drds,\ \iint \frac{1}{R_a^3}drdy,\ \iint \frac{1}{R_a^3}dsdy, \\ & \int \frac{1}{R_a}dy,\ \int \frac{1}{R_a}dr,\ \int \frac{1}{R_a}ds \end{aligned} \tag{25}$$

We were successful in finding an analytical solution for all cases except the triple integral $\iiint \frac{1}{R_a^3}drdsdy$. Irrespective of the order of integration, the first two integrations lead to a convoluted arctangent function. Since this function is continuous and well behaved as long as $a > 0$, an antiderivative should exist, but we have not found any analytical form for it. However, as was the case for the quadrangle, this seed integral actually cancels out in the recurrence relations and does not impact the final nodal force evaluation. Therefore, its value is simply set to zero and the proposed methodology remain fully analytical.

Thanks to the recurrence form of all required (simple, double and triple) integrals, the nodal force can be seen as -a long- sum of terms where intermediate integrals and initial seed functions are multiplied by polynomials $r^i s^j y^k$. This property will be particularly interesting when deriving a solution for a semi-infinite segment.

In total, the change from a linear quadrangle to a quadratic triangle significantly increases the amount of work and the number of integrals required, with four new types of integrals needed to handle the new definition for the r and s integral bounds, and additional dozens of integrals related to the quadratic form of the shape functions.

Extension of the model to the semi-infinite segment

In the case of a finite domain containing dislocations that terminate at the domain boundaries, the stress field associated with such open-loop microstructure may not be divergence free, even after superimposing the corrective field [14, 15]. One solution could be to use the rational stress expression proposed by Asano [23], which remains divergent free even in the case of open loops. Here, we propose a more practical solution that consists in "closing" the open microstructure by adding virtual semi-infinte segments in the infinite domain [14, 15, 7]. The extension of our approach to the case of a semi-infinite piercing segment is presented hereafter.

We now consider a piercing semi-infinite segment where the node $\mathbf{x_1}$ is on the triangular element and the node $\mathbf{x_2}$ is sent to $+\infty$. This corresponds to a finite value for bound y_1 of the scalar y that spans the dislocation segment, while y_2 tends to $+\infty$ in the line integral 4. Non-singular stress expressions $\sigma^{(\mathbf{x_1}+\infty)}$ for the semi-infinite segment can be found in [16]. Since, the stress field induced by a semi-infinite non-singular segment is defined and finite everywhere, the corresponding traction field $\sigma^{(\mathbf{x_1}+\infty)} \cdot \mathbf{n}$ is also defined and finite on a finite surface element. However, particular attention should be paid to the way in which the y_2 integral bound is handled. The triple integrals required for the derivation of the nodal traction now read:

$$\int\int\int_{y_1}^{+\infty} \frac{r^i s^j y^k}{R_a^l} dr ds dy = \left[\iint F(r,s,+\infty) dr ds\right]_{+\infty} - \left[\iint F(r,s,y_1) dr ds\right]_{y_1}$$

Where, F are the antiderivatives of $\int \frac{r^i s^j y^k}{R_a^l} dy$. These integrals can still be obtained by means of the same recurrence relations derived for the finite segments that remain valid for the semi-infinite case. However, it is necessary to determine the asymptotic behaviour of the first term in the right hand side of equation 26 as $y_2 \to +\infty$. Since triple integrals correspond to a long sum of terms multiplied by polynomials of the form $r^i s^j y^k$, and recalling that the limit of a convergent sum is the sum of the limits, we must simply investigate the asymptotic behavior of the seed functions as as $y_2 \to +\infty$. Integration with respect to y, is associated to integration constants of the form $C(r,s)$. However, as the integration path remains the same for the nodes $\mathbf{x_2}$ and $\mathbf{x_1}$, the integration constants will cancel out in the final sum.

Since the seed functions are convoluted functions of y_2, the asymptotic behaviour of these functions is determined by means of Taylor expansions and by using the simple change of variable $\lambda = \frac{1}{y_2}$. The order of the Taylor expansion is adapted according to the power of y_2 applied in front of the seed function in order to maintain an overall error term as $O\left(\frac{1}{y_2}\right)$ or smaller. Since the error terms are vanishing as $y_2 \to +\infty$, the nodal force induced by a semi-infinite segment is finite and the proposed approach can be regarded as exact in the limit sense. Details of this derivation can be found in Appendix B.

Comparison with a conventional quadrature procedure

Great care has been paid to the implementation and validation of the model into C and Matlab routines. One of the difficulty in this implementation is related to the large number of intermediate integrals that need to be calculated prior to the final evaluation of the nodal forces and the corresponding triple integrals. The recurrence form of the solution is particularly well adapted to an implementation by means of nested loops on indices i, j, k and j as suggested in [18]. All integrals have been individually checked and validated by the comparison with a conventional quadrature procedure and large number of quadrature points. The code files will be freely distributed upon request to the corresponding author.

This section focuses now on the comparison of the proposed analytical evaluation of nodal forces with a more conventional quadrature procedure to evaluate the integrals. Quadrature methods are very versatile but may not be particularly well adapted to fast spatially varying field like the stress field of dislocations, even in the case of the non-singular theory. This comparison will be the occasion to validate our practical implementation into code form of the model and to discuss when it is better to use one method over the other.

For this comparison, we employ two successive Gauss-Legendre quadrature [24] to approximate the nodal force on node (n) as:

$$\mathbf{F}^{(n)} \approx \sum_{i=1}^{M} w_i \sum_{j=1}^{M} w_j \left[\sigma^{(x_1 x_2)}(r_i, s_j)\cdot\mathbf{n}\right] N^{(n)}(r_i, s_j) \tag{26}$$

where, r_i and s_j are the locations along $\mathbf{p}$ and $\mathbf{q}$ where the function $[\sigma^{(x_1x_2)}(\mathbf{x})\cdot\mathbf{n}]\, N^{(n)}(\mathbf{x})$ is being evaluated and w_i and w_j are weighting functions. Values for the reduced abscissas r_i and w_i can be found in [24] as a function of the number of quadrature points M. Here, the stress field $\sigma^{(x_1x_2)}$ corresponds to the one from a finite or semi-infinite segment and use is made of the analytical expressions provided in [25, 16].

The configuration considered for the comparison is as follows. The isotropic elastic constants are those for pure α-iron with $\mu = 63.5$ GPa and $\nu = 0.333$ [26]. A dislocation segment of length 400 $|\mathbf{b}|$ is placed at a varying distance D from a triangular element with a side of 4000 $|\mathbf{b}|$, where $|\mathbf{b}| = 2.48\mathring{A}$. The core spreading a can dramatically smooth the stress concentration close to the core of dislocations when its value is set to large values leading to rather unphysical situations. Here, we use the widely used and realistic value of $a = 1|\mathbf{b}|$ [27].

Figure 3 displays the relative error associated to the Gauss quadrature as a function of the number of Quadrature Points (QP) M^2. Interestingly, for fixed segment and element dimensions, the relative error associated to the Gauss quadrature when compared to the present analytical work mostly depends upon the character of the dislocation and the separation distance between the dislocation segment and the surface element. As expected, the relative error decreases as the number of QP is increased until reaching a value close to 10^{-12} corresponding to the double precision limit of floating

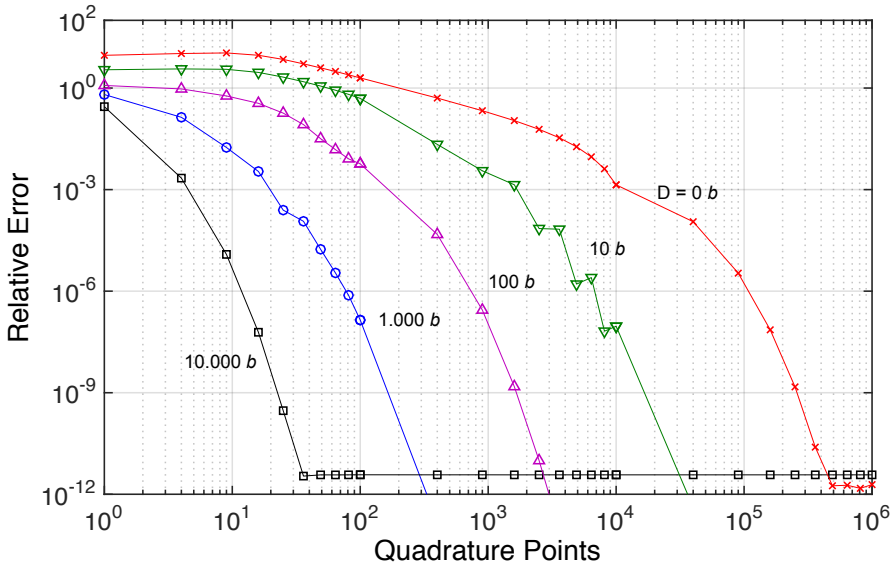

Figure 3. Evaluation of the numerical error associated with a Gauss-Legendre Quadrature of the nodal force as a function of the number of QPs and the distance D separating the dislocation segment and the surface element. The quadratic six node element exhibits two random oriented sides of length 4000 $|\mathbf{b}| \approx 1\mu$m, the segment is also randomly oriented and has an edge character.

point format. However, the "speed" at which the relative error decreases depends upon the separation distance between the dislocation segment and the surface element. As an illustration, targeting a precision of 10^{-4} or better would require to use 6 QP when the dislocation segment is as far as 10,000 b from the element, to use 200 QP at a 100 b from the element, and 30,000 QP for a piercing segment. Next, we compare the computational cost associated with our analytical approach and with the numerical quadrature.

To discuss and compare the numerical cost of the two approaches, we introduce a reference numerical cost that will help in assessing the overhead associated with the double integration upon the surface element alone. For this, we chose the cost associated with one stress at a point evaluation as a reference cost. The evaluation of the stress induced by a single dislocation can be made using analytical expressions for the finite segment [25]. Our analytical method is associated with a fixed numerical cost of 4.5 times a single stress at a point evaluation. Figure 4 shows the evolution of the numerical cost associated with Gauss quadrature with respect to the number of QP. The cost starts at a very small value but increases rather quickly with the number of QPs.

Finally, when comparing with our previous work on linear quadrangle, a number of observations can be made. As stated in the beginning of the paper, the extra effort required to go from linear elements to quadratic arbitrary shaped triangles is considerable, as all recurrence relations and analytical integrals must be done from scratch. Unexpectedly, the numerical cost associated with our new analytical approach is slightly lower than the cost of our previous work, which is probably due to a difference

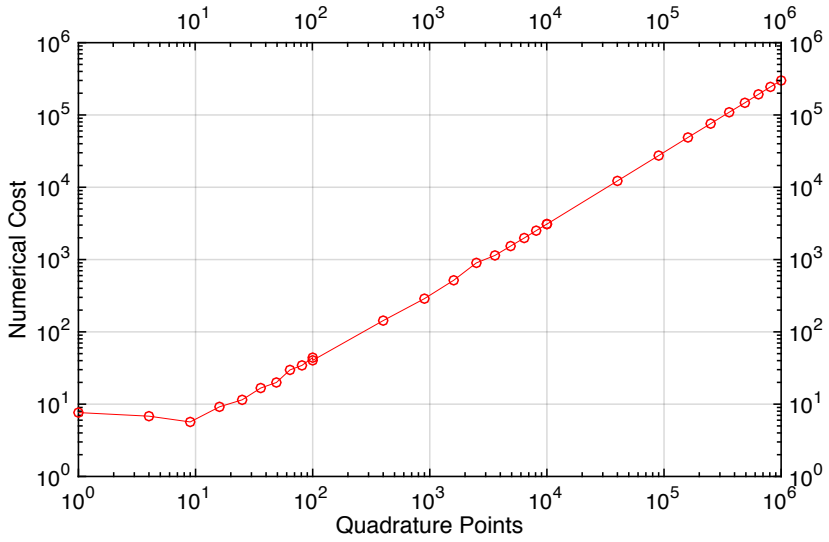

Figure 4. Evaluation of the cost associated with the Gauss-Legendre Quadrature of the nodal force as a function of the number of QPs. The numerical cost is relative to the cost of a single stress at a point evaluation.

and more efficient implementation of the recurrence relations. The Gauss quadrature seems to converge towards our analytical work faster that in the case of the linear quadrangle, this could be due to the additional higher-order terms required as Gauss quadrature tends to offer a better approximation of polynomials. From a more practical standpoint, our choice of approach should be based a compromise between accuracy and speed. The easy-to-use and versatile Gauss quadratures could be used to evaluate tractions of segments of dislocations that are far from the boundaries, but attention must be paid to the evaluation of the associated numerical errors that may quickly reach unacceptable levels. For segments close to or in contact with surface elements, Gauss quadrature requires a large numbers of QP to remain accurate and therefore becomes rather inefficient numerically.

Acknowledgements

References

[1] E. Van der Giessen and A. Needleman. Discrete dislocation plasticity: a simple planar model. *Modelling Simul. Mater. Sci. Eng.*, 3(5):689–735, September 1995.

[2] C. Lemarchand, B. Devincre, and L. P. Kubin. Homogenization method for a discrete-continuum simulation of dislocation dynamics. *Journal of the Mechanics and Physics of Solids*, 49(9):1969–1982, September 2001.

[3] R Martinez and N M Ghoniem. The Influence of Crystal Surfaces on Dislocation Interactions in Mesoscopic Plasticity: A Combined Dislocation Dynamics- Finite Element Approach. *Comput. Modeling Eng. Sci.*, 3:229–43, 2002.

[4] Hussein M. Zbib, Tomas Diaz de la Rubia, and Vasily Bulatov. A Multiscale Model of Plasticity Based on Discrete Dislocation Dynamics. *J. Eng. Mater. Technol*, 124(1):78–87, May 2001.

[5] M. P. O'Day and W. A. Curtin. A Superposition Framework for Discrete Dislocation Plasticity. *Journal of Applied Mechanics*, 71(6):805, 2004.

[6] Meijie Tang, Wei Cai, Guanshui Xu, and Vasily V. Bulatov. A hybrid method for computing forces on curved dislocations intersecting free surfaces in three-dimensional dislocation dynamics. *Modelling Simul. Mater. Sci. Eng.*, 14(7):1139–1151, August 2006.

[7] Christopher R. Weinberger, Sylvie Aubry, Seok-Woo Lee, William D. Nix, and Wei Cai. Modelling dislocations in a free-standing thin film. *Modelling Simul. Mater. Sci. Eng.*, 17(7):075007, August 2009.

[8] A. Vattré, B. Devincre, F. Feyel, R. Gatti, S. Groh, O. Jamond, and A. Roos. Modelling crystal plasticity by 3d dislocation dynamics and the finite element method: The Discrete-Continuous Model revisited. *Journal of the Mechanics and Physics of Solids*, 63:491–505, February 2014.

[9] O. Jamond, R. Gatti, A. Roos, and B. Devincre. Consistent formulation for the Discrete-Continuous Model: Improving complex dislocation dynamics simulations. *International Journal of Plasticity*, 80:19–37, May 2016.

[10] M. Stricker, J. Gagel, S. Schmitt, K. Schulz, D. Weygand, and P. Gumbsch. On slip transmission and grain boundary yielding. *Meccanica*, 51(2):271–278, February 2016.

[11] Jaafar A. El-Awady, S. Bulent Biner, and Nasr M. Ghoniem. A self-consistent boundary element, parametric dislocation dynamics formulation of plastic flow in finite volumes. *Journal of the Mechanics and Physics of Solids*, 56(5):2019–2035, May 2008.

[12] Joshua C Crone, Peter W Chung, Kenneth W Leiter, Jaroslaw Knap, Sylvie Aubry, Gregg Hommes, and Athanasios Arsenlis. A multiply parallel implementation of finite element-based discrete dislocation dynamics for arbitrary geometries. *Modelling and Simulation in Materials Science and Engineering*, 22(3):035014, April 2014.

[13] N. Bertin and L. Capolungo. A FFT-based formulation for discrete dislocation dynamics in heterogeneous media. *Journal of Computational Physics*, 355:366–384, February 2018.

[14] D. Weygand, L. H. Friedman, E. Van der Giessen, and A. Needleman. Aspects of boundary-value problem solutions with three-dimensional dislocation dynamics. *Modelling Simul. Mater. Sci. Eng.*, 10(4):437–468, June 2002.

[15] J. Deng, A. El-Azab, and B. C. Larson. On the elastic boundary value problem of dislocations in bounded crystals. *Philosophical Magazine*, 88(30-32):3527–3548, October 2008.

[16] S Queyreau, J Marian, B D Wirth, and A Arsenlis. Analytical integration of the forces induced by dislocations on a surface element. *Modelling and Simulation in Materials Science and Engineering*, 22(3):035004, April 2014.

[17] W Cai, A Arsenlis, C Weinberger, and V Bulatov. A non-singular continuum theory of dislocations. *Journal of the Mechanics and Physics of Solids*, 54(3):561–587, March 2006.

[18] B. Liu, A. Arsenlis, and S. Aubry. Computing forces on interface elements exerted by dislocations in an elastically anisotropic crystalline material. *Modelling Simul. Mater. Sci. Eng.*, 24(5):055013, June 2016.

[19] Toshio Mura. Dislocations. In *Micromechanics of defects in solids*, pages 277–333. Springer Netherlands, Dordrecht, 1982.

[20] S Aubry and A Arsenlis. Use of spherical harmonics for dislocation dynamics in anisotropic elastic media. *Modelling and Simulation in Materials Science and Engineering*, 21(6):065013, September 2013.

[21] Giacomo Po, Markus Lazar, Dariush Seif, and Nasr Ghoniem. Singularity-free dislocation dynamics with strain gradient elasticity. *Journal of the Mechanics and Physics of Solids*, 68:161–178, August 2014.

[22] David V. Hutton. *Fundamentals of Finite Element Analysis*. McGraw-Hill, 2004.

[23] Shigeru Asano. Stress Tensor of a Finite Dislocation. *J. Phys. Soc. Jpn.*, 25(1):220–226, July 1968.

[24] William H. Press, Saul A. Teukolsky, William T. Vetterling, and Brian P. Flannery. *Numerical Recipes 3rd Edition: The Art of Scientific Computing*. Cambridge University Press, New York,

NY, USA, 3 edition, 2007.

[25] A. Arsenlis, W. Cai, M. Tang, M. Rhee, T. Oppelstrup, G. Hommes, T. G. Pierce, and V. V. Bulatov. Enabling strain hardening simulations with dislocation dynamics. *Modelling Simul. Mater. Sci. Eng.*, 15(6):553–595, July 2007.

[26] John Price Hirth and Jens Lothe. *Theory of Dislocations*. Krieger Publishing Company, 1982.

[27] Derek Hull and D. J. Bacon. *Introduction to dislocations*. Butterworth-Heinemann, Oxford, 4th ed edition, 2001.